Journal of Materials Chemistry B

PAPER

View Article Online
View Journal | View Issue

Cite this: J. Mater. Chem. B, 2019, 7, 2434

An AIE-active theranostic probe for light-up detection of Aβ aggregates and protection of neuronal cells†

Yaqi Yang,‡[a] Shiwu Li,‡[b] Qin Zhang,[a] Ying Kuang,[a] Anjun Qin,[b] Meng Gao,*[c] Feng Li*[a] and Ben Zhong Tang*[bde]

Received 19th January 2019,
Accepted 1st March 2019

DOI: 10.1039/c9tb00121b

rsc.li/materials-b

Alzheimer's disease (AD) is one of the most serious health threats in our aging society. The major pathological feature of AD is excessive extracellular aggregation of β-amyloid (Aβ) protein in the form of Aβ fibrils or plaques. The simultaneous detection of Aβ fibrils and inhibition of their neurotoxicity is highly desirable for study of Alzheimer's disease. Although various fluorophores have been developed for imaging of Aβ fibrils or plaques, they suffer from serious self-quenching at high concentration and a lack of neuroprotective functions. To tackle these challenges, we herein develop a multi-functional probe of Cur-N-BF_2 with aggregation-induced emission (AIE) characteristics for light-up detection of Aβ fibrils and plaques, inhibition of Aβ fibrillation, disassembly of preformed Aβ fibrils, and protection of neuronal cells. The AIE-active theranostic probe is thus promising for study of Aβ fibrils and plaques in Alzheimer's disease.

Introduction

Alzheimer's disease (AD) is one of the most serious health threats in our aging society.[1] One major pathological feature of AD is an excessive extracellular aggregation of β-amyloid (Aβ) protein in the form of Aβ fibrils or plaques, which would trigger the activation of neurotoxic cascades and lead to neuronal dysfunction.[2] It is thus highly desirable to develop theranostic probes for simultaneous detection of Aβ fibrils and inhibition of their neurotoxicity. Although various imaging techniques have been developed for detection of Aβ fibrils or plaques, such as positron emission tomography (PET),[3] single photon emission computed tomography (SPECT),[4] and magnetic resonance imaging (MRI),[5] they suffer from high cost, radioactivity, and low sensitivity.[6] Compared with these imaging techniques, fluorescence imaging has the advantages of low cost, high resolution, and excellent sensitivity. In the last decade, a variety of fluorophores have been developed for imaging of Aβ aggregates, such as Thioflavin T (ThT), Thioflavin S (ThS), oxazines, BODIPYs, and stilbenes.[7] However, these fluorophores may suffer from aggregation-caused quenching (ACQ) drawbacks and their accumulation at Aβ aggregate sites would lead to serious self-quenching.[8] For example, the commercial ThT would undergo serious self-quenching after binding with Aβ fibrils at a high concentration.[8b]

In contrast with the ACQ fluorophores, aggregation-induced emission fluorogens (AIEgens) feature high emission efficiency in the aggregate state, strong photo-stability, and excellent biocompatibility.[9] Based on these unique advantages, AIEgens have found broad applications in bio-imaging.[10] For example, several TPE derivatives have been developed for monitoring of the fibrillation process of insulin and β-amyloid proteins with a high signal-to-noise ratio.[11] However, multi-functional AIEgens are highly desirable, which can not only be used for light-up detection of Aβ fibrils, but also can protect neuronal cells from the damage of Aβ fibrils.

Curcumin has been widely investigated for selective imaging of Aβ aggregates and inhibition of the growth of Aβ fibrils,[12] and several curcumin derivatives have been developed to

[a] Guangdong Provincial Key Laboratory of Brain Function and Disease, Department of Neurobiology and Anatomy, Zhongshan School of Medicine, Sun Yat-sen University, Guangzhou 510080, China. E-mail: lifeng@mail.sysu.edu.cn
[b] State Key Laboratory of Luminescent Materials and Devices, Center for Aggregation-Induced Emission, Guangzhou International Campus, South China University of Technology, Guangzhou, 510640, China
[c] National Engineering Research Center for Tissue Restoration and Reconstruction, South China University of Technology, Guangzhou, 510006, China. E-mail: msmgao@scut.edu.cn
[d] HKUST-Shenzhen Research Institute, Shenzhen, 518057, China
[e] Department of Chemistry, Hong Kong Branch of Chinese National Engineering Research Centre for Tissue Restoration and Reconstruction, Institute for Advanced Study, and Department of Chemical and Biological Engineering, The Hong Kong University of Science & Technology, Clear Water Bay, Kowloon, Hong Kong, China. E-mail: tangbenz@ust.hk

† Electronic supplementary information (ESI) available: Structural characterization of Cur-N-BF_2, cytotoxicity, $A\beta_{1-42}$ fibrillation monitoring, TEM, hemolysis test, and statistical analysis. See DOI: 10.1039/c9tb00121b

‡ Y. Yang and S. Li contributed equally to this work.

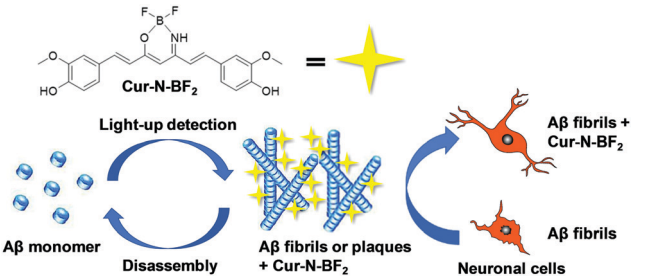

Scheme 1 The AIE-active probe Cur-N-BF_2 for light-up detection of Aβ fibrils and plaques, inhibition of Aβ fibrillation, disassembly of Aβ fibrils, and protection of neuronal cells.

improve the signal-to-noise ratio for imaging of Aβ fibrils. However, most of the curcumin derivatives for imaging of Aβ fibrils suffer from ACQ drawbacks.[13] To tackle this challenge, we herein develop a multifunctional AIE-active probe Cur-N-BF_2 for light-up detection of Aβ fibrils and plaques, inhibition of Aβ fibrillation, disassembly of preformed Aβ fibrils, and efficient protection of neuronal cells from the damage of Aβ fibrils (Scheme 1).

Results and discussion

Synthesis and photophysical characterization

The synthetic routes of Cur-N-BF_2 and Cur-O-BF_2 are shown in Scheme 2. The reaction of curcumin with ammonium formate first generated Cur-NH_2 in 53% yield, which further reacted with $BF_3{\cdot}Et_2O$ to afford Cur-N-BF_2 in 31% yield. Meanwhile, Cur-O-BF_2 was prepared through the direct reaction of curcumin with $BF_2{\cdot}Et_2O$.[14] All these compounds were well characterized and unambiguously verified by NMR and HRMS analysis (Fig. S1–S3, ESI†).

The photophysical properties of Cur-N-BF_2 and Cur-O-BF_2 were then investigated. In THF solution, Cur-N-BF_2 showed maximum absorption at 427 nm, while Cur-O-BF_2 showed red-shifted absorption at 501 nm (Fig. 1A and B). Both Cur-N-BF_2 and Cur-O-BF_2 showed greatly enhanced fluorescence in the solid state compared to in aqueous solution, which was verified by the PL spectra and quantum yield measurement (Fig. 1C and D). In the solid state, Cur-N-BF_2 showed maximum emission at 572 nm with a quantum yield of 14.0%, while Cur-O-BF_2 showed maximum emission at 655 nm with a much lower quantum yield of 1.2%. The HOMOs and LUMOs of

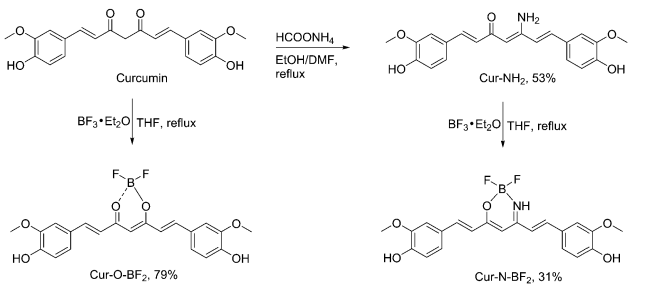

Scheme 2 Synthetic routes of Cur-N-BF_2 and Cur-O-BF_2.

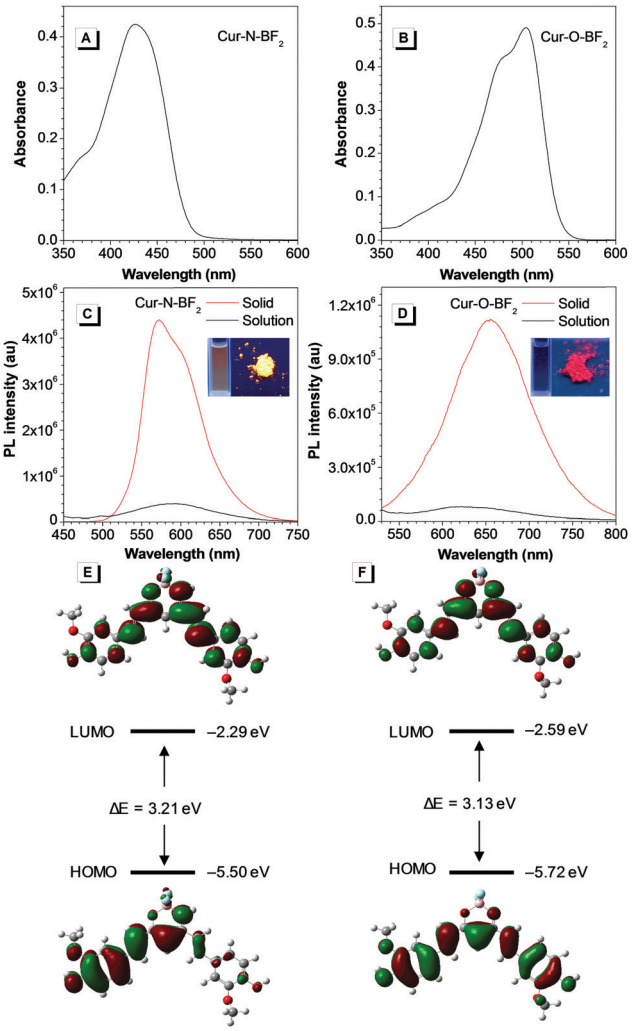

Fig. 1 The UV-vis absorption spectra of (A) Cur-N-BF_2 and (B) Cur-O-BF_2 in THF solution; the PL spectra of (C) Cur-N-BF_2 and (D) Cur-O-BF_2 in the solid state and in aqueous solution; [Cur-N-BF_2] = [Cur-O-BF_2] = 10 μM; for Cur-N-BF_2, λ_{ex} = 427 nm; for Cur-O-BF_2, λ_{ex} = 501 nm; inset: the photographs of Cur-N-BF_2 and Cur-O-BF_2 in aqueous solution (left) and the solid state (right) under UV irradiation at 365 nm. The optimized molecular orbital amplitude plots of the HOMOs and LUMOs of (E) Cur-N-BF_2 and (F) Cur-O-BF_2.

Cur-N-BF_2 and Cur-O-BF_2 were then calculated based on density functional theory (Fig. 1E and F), and a higher energy gap was obtained for Cur-N-BF_2 (3.21 eV) compared to Cur-O-BF_2 (3.13 eV). The HOMO orbital of Cur-N-BF_2 is mainly localized on the oxygen atom side, which could be due to the higher electronegativity of the oxygen than the nitrogen atom.[15]

We further measured the PL spectra of Cur-N-BF_2 and Cur-O-BF_2 in a THF/water mixture, which showed a bathochromic shift of the emission and decreased intensity with increasing water fraction (Fig. S4, ESI†). This could be due to their strong donor–acceptor structural features and the twisted intramolecular charge transfer (TICT) effect.[16] Their emission spectra are also closely correlated with the environmental viscosity. A 4- and 5-fold emission enhancement was respectively observed for Cur-N-BF_2 and Cur-O-BF_2 in glycerol (η = 945 mPa S)

compared to in methanol (η = 0.59 mPa S) (Fig. S5, ESI†),[17] which could be due to the restriction of intramolecular motion (RIM) in high viscosity media.[18]

Biocompatibility of Cur-N-BF_2

Based on MTT assay, we evaluated the cytotoxicities of Cur-N-BF_2, Cur-O-BF_2, curcumin, and ThT with mouse hippocampal neuronal cells (HT22 cells) as a model cell line. The cell viability was ~100%, 37.8%, 75.6%, and 45.2% in the presence of 20 μM Cur-N-BF_2, Cur-O-BF_2, curcumin, and ThT, respectively (Fig. S6A, ESI†). These results suggest that Cur-N-BF_2 is much less cytotoxic than Cur-O-BF_2 and the commercial staining agents of curcumin and ThT. We also investigated the cytotoxicity of Cur-N-BF_2 with human neuroblastoma SHSY5Y cells and rat pheochromocytoma PC12 cells (Fig. S6B, ESI†), which showed nearly ~100% viability in the presence of Cur-N-BF_2 at 20 μM. We then conducted the hemolysis test to evaluate the biocompatibility of Cur-N-BF_2. The hemolytic ratio was only 1.29% with Cur-N-BF_2 at 500 μM (Fig. S6C, ESI†), which is much lower than the safety limit (5%).[19]

Light-up detection of $A\beta_{1-42}$ fibrils

We then investigated the detection abilities of Cur-N-BF_2, curcumin, and ThT for $A\beta_{1-42}$ fibrils. The $A\beta_{1-42}$ fibrils were prepared from $A\beta_{1-42}$ peptide by incubation in PBS at 37 °C for 0, 1, 4, and 7 days, respectively (Fig. S7, ESI†).[20] After addition of Cur-N-BF_2, increased fluorescence was observed for the samples with longer incubation time (Fig. 2A), which can be ascribed to the binding of Cur-N-BF_2 with the hydrophobic domains of $A\beta_{1-42}$ fibrils to restrict the intramolecular motion and inhibit the TICT effect.[11] We then investigated the light-up detection abilities of Cur-N-BF_2, curcumin, and ThT at different concentrations. An increased fluorescence intensity was observed for Cur-N-BF_2 even at a high concentration (4.0 mM) (Fig. 2B and Fig. S8, ESI†). Meanwhile, both curcumin and ThT underwent serious self-quenching when their concentrations exceeded 0.05 and 0.25 mM, respectively (Fig. 2C and D). The Cur-N-BF_2 probe is thus superior to the commercial curcumin and ThT, which suffer from the ACQ effect. We also screened a series of proteins to verify the selectivity of Cur-N-BF_2 for $A\beta_{1-42}$ fibrils, including human serum albumin (HSA), transferrin, insulin, lysozyme, pepsin, and trypsin. Only Aβ fibrils could significantly light-up the fluorescence of Cur-N-BF_2 (Fig. S9, ESI†), which suggests the probe could be used for selective detection of Aβ fibrils.

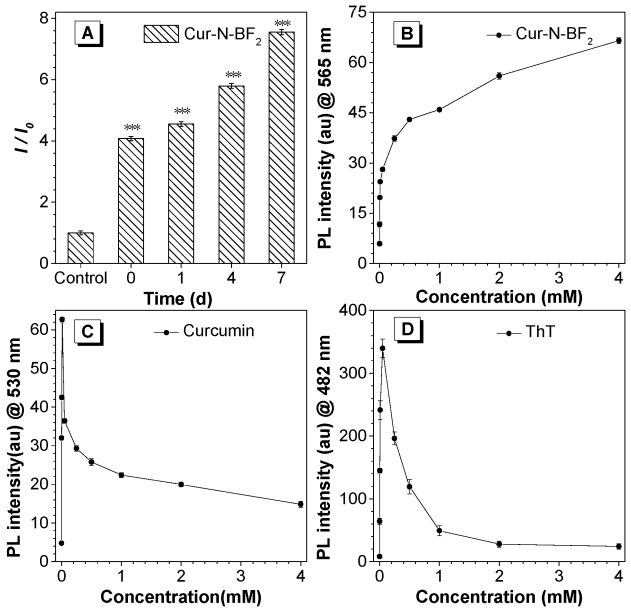

Fig. 2 (A) The PL intensity changes (I/I_0) of Cur-N-BF_2 at 565 nm for detection of $A\beta_{1-42}$ fibrils formed at 0, 1, 4, and 7 days, respectively; λ_{ex} = 426 nm; [Cur-N-BF_2] = 10 μM, [$A\beta_{1-42}$] = 50 μM, ***$P < 0.001$; (B–D) in the presence of $A\beta_{1-42}$ fibrils (20 μM), the PL intensity changes with increasing concentrations of Cur-N-BF_2, curcumin, and ThT; for Cur-N-BF_2, λ_{ex} = 426 nm, λ_{em} = 565 nm; for curcumin, λ_{ex} = 425 nm, λ_{em} = 530 nm; for ThT, λ_{ex} = 430 nm, λ_{em} = 482 nm.

Selective staining of Aβ plaques in brain slices

The selective staining ability of Cur-N-BF_2 for Aβ plaques was then investigated with brain slices from plaque-rich APPswe/PSEN1dE9 transgenic mice (APP/PS1).[21] The Aβ plaques on the hippocampus and cerebral cortex could be clearly observed with a high signal-to-noise ratio by staining with Cur-N-BF_2 (Fig. 3A and E). The high selectivity of Cur-N-BF_2 for Aβ plaques was well verified by co-staining with the commercial staining agent of β-amyloid antibody (Fig. 3B and F) and an excellent overlap coefficient of 0.93 and 0.89 was respectively obtained for hippocampus and cerebral cortex slices (Fig. 3C, G and Fig. S10, ESI†). Moreover, a high signal synchrony was observed for the region of interest (ROI) across the plaque region (Fig. 3D and H). Moreover, Cur-N-BF_2 could be directly used for wash-free imaging of Aβ plaques with a high signal-to-noise ratio (Fig. S11A–D, ESI†), while a strong background noise was observed for β-amyloid antibody without washing (Fig. S11E–H, ESI†). The brain slice obtained from wild-type mice (C57BL/6) was also stained with Cur-N-BF_2 as a comparison and no obvious fluorescence signal was observed, which further verified the selectivity of Cur-N-BF_2 for Aβ plaques (Fig. S12, ESI†).[22]

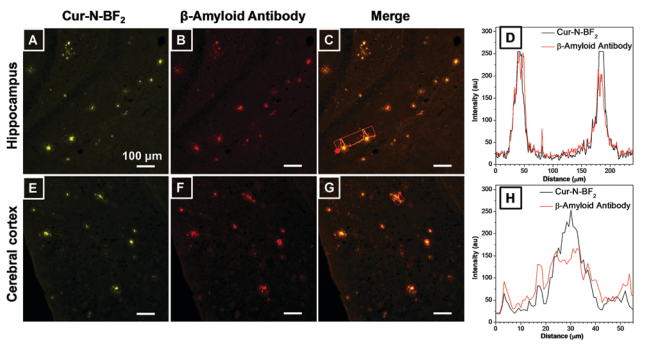

Fig. 3 The CLSM images of hippocampus and cerebral cortex slices obtained from APP/PS1 mice and stained with (A and E) Cur-N-BF_2 (100 μM) and (B and F) β-amyloid antibody (Cell Signaling Technology, 1:200); (C and G) the merged images; (D and H) the intensity profile of ROI lines. Scale bar = 100 μm.

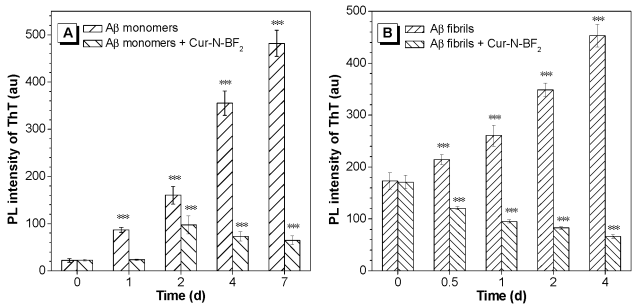

Fig. 4 The ThT fluorescence assay for monitoring the formation and disassembly of $A\beta_{1-42}$ fibrils. (A) The monomeric $A\beta_{1-42}$ peptides (20 μM) were incubated with Cur-N-BF_2 (10 μM) for 0, 1, 2, 4, and 7 days; (B) the $A\beta_{1-42}$ fibrils (20 μM) formed at day 2 were incubated with and without Cur-N-BF_2 (10 μM) for 0.5, 1, 2, and 4 days at 37 °C; [ThT] = 10 μM; ***$P < 0.001$.

Inhibition of Aβ fibrillation and disassembly of Aβ fibrils

Based on ThT fluorescence assay, we then investigated whether Cur-N-BF_2 could inhibit $A\beta_{1-42}$ fibrillation and promote the disassembly of $A\beta_{1-42}$ fibrils.[23] After incubation with $A\beta_{1-42}$ peptide (20 μM) at 37 °C for 7 days (Fig. 4A), a much lower light-up ratio of 3-fold was observed for the ThT assay in the presence of Cur-N-BF_2 (10 μM) than that without Cur-N-BF_2 (22-fold), which suggests that the formation of $A\beta_{1-42}$ fibrils could be efficiently inhibited by Cur-N-BF_2. Moreover, a gradually decreased fluorescence intensity was observed for the ThT assay after addition of Cur-N-BF_2 into the $A\beta_{1-42}$ fibril solution (Fig. 4B), while the ThT fluorescence intensity continued to increase in the absence of Cur-N-BF_2. These results suggest that Cur-N-BF_2 could not only inhibit the formation of Aβ fibrils, but also could promote the disassembly of preformed $A\beta_{1-42}$ fibrils.

We then conducted transmission electron microscopy (TEM) to investigate the morphology changes of Aβ aggregates.[24] After incubation of 20 μM $A\beta_{1-42}$ peptide at 37 °C for 2 days (Fig. 5A), many short and branched Aβ protofibrils were observed. After further incubation at 37 °C for 4 days, the $A\beta_{1-42}$ peptide formed a filamentous and branching network with abundant mature fibrils (Fig. 5B). In contrast, the Aβ protofibrils dissembled into spherical and amorphous aggregates after further incubation with 10 μM Cur-N-BF_2 for 4 days (Fig. 5C). We further measured the circular dichroism (CD) spectra to investigate the conformational changes of $A\beta_{1-42}$ aggregates.[25] As shown in Fig. 5D, after incubation of $A\beta_{1-42}$ peptide for 6 days, an obviously negative CD band at 218 nm was observed, which is a characteristic of β-sheet structure.[26] Meanwhile, the incubation of $A\beta_{1-42}$ in the presence of Cur-N-BF_2 for 6 days led to a much lower CD intensity at 218 nm, which suggests that Cur-N-BF_2 could efficiently inhibit the formation of β-sheet structure. The TEM images and CD spectra are consistent with the ThT assay results, which clearly verified that Cur-N-BF_2 could efficiently inhibit Aβ fibrillation and promote disassembly of Aβ fibrils.

Protection of neuronal cells from the toxicity of Aβ fibrils

We then investigated the neuronal cell protection ability of Cur-N-BF_2 with HT22 cells as a model cell line.[27] By immunofluorescent staining of microtubules with anti-tubulin antibody, an obvious cell shrinkage and decrease of the neurite extension were observed for HT22 cells treated with 40 μM $A\beta_{1-42}$ fibrils for 36 h (Fig. 6A–H) and the cell viability decreased to 55.5% (Fig. S13A, ESI†). After further incubation with 10 μM Cur-N-BF_2 for 24 h, the cells recovered their normal morphology (Fig. 6I–L) and the cell viability increased to 83.2% (Fig. S13B, ESI†). These results suggest that Cur-N-BF_2 could efficiently protect HT22 neuronal cells from the toxicity of Aβ fibrils.

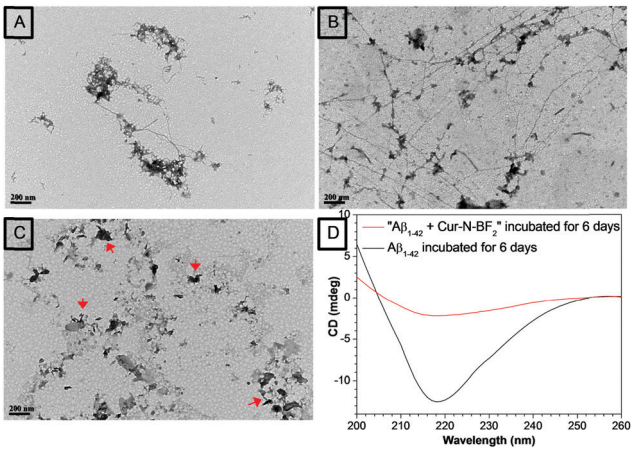

Fig. 5 The TEM images of $A\beta_{1-42}$ aggregates after incubation of $A\beta_{1-42}$ peptide at 37 °C for (A) 2 days; (B) 6 days; and (C) 6 days in the presence of Cur-N-BF_2; arrowheads indicate clusters of spherical structures; (D) the CD spectra of $A\beta_{1-42}$ peptide after incubation at 37 °C for 6 days in the presence and absence of Cur-N-BF_2; [$A\beta_{1-42}$] = 20 μM, [Cur-N-BF_2] = 10 μM. Scale bar = 200 nm.

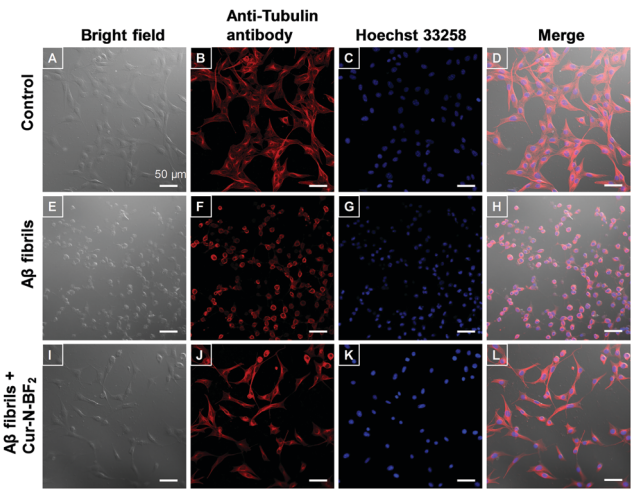

Fig. 6 The morphology changes of HT22 cells: (A–D) under the control; (E–H) treated with $A\beta_{1-42}$ fibrils; (I–L) treated with $A\beta_{1-42}$ fibrils for 36 h, and then treated with Cur-N-BF_2 for 24 h; [$A\beta_{1-42}$ fibrils] = 40 μM; [Cur-N-BF_2] = 10 μM; scale bar = 50 μm.

Conclusions

In summary, we develop a multifunctional AIE-active probe Cur-N-BF_2 for light-up detection of Aβ fibrils and plaques,

protection of neuronal cells by inhibition of Aβ fibrillation, and disassembly of the preformed Aβ fibrils. Compared with the commercial Aβ staining agents, the AIE-active Cur-N-BF_2 has significant advantages in terms of easy preparation, high selectivity, and direct imaging of Aβ plaques with a high signal-to-noise ratio and without self-quenching drawbacks. The excellent neuronal cell protection ability of Cur-N-BF_2 further makes it promising as a theranostic agent in the study of Alzheimer's disease.

Experimental

Synthesis of Cur-NH_2

Curcumin (1.10 g, 3.0 mmol) and ammonium formate (1.16 g, 15 mmol) were dissolved in a mixture of ethanol (30 mL) and dimethyl formamide (5 mL). The mixture was then heated under reflux under nitrogen overnight. After completion of the reaction, the mixture was cooled to room temperature and evaporated under reduced pressure. The residue was extracted with dichloromethane (50 mL × 3) and the combined organic layers were dried over anhydrous $MgSO_4$ and concentrated under reduced pressure. The product was then purified by silica gel column chromatography using dichloromethane as the eluent to afford a yellow solid of Cur-NH_2 in 53% yield (587 mg). ^{1}H NMR (DMSO-d_6, 500 MHz): δ 9.84 (br s, 1H), 9.45 (br s, 2H), 7.50 (br s, 1H), 7.28–7.37 (m, 2H), 7.23 (d, J = 2.0 Hz, 1H), 7.18 (d, J = 2.0 Hz, 1H), 7.05 (dd, J_1 = 8.0 Hz, J_2 = 2.0 Hz, 1H), 6.98 (dd, J_1 = 8.5 Hz, J_2 = 2.0 Hz, 1H), 6.78–6.82 (m, 2H), 6.70 (d, J = 15.5 Hz, 1H), 6.52 (d, J = 16.0 Hz, 1H), 5.50 (s, 1H), 3.83 (s, 3H), 3.82 (s, 3H); ^{13}C NMR (DMSO-d_6, 125 MHz): δ 186.3, 158.8, 148.2, 148.0, 147.8, 137.3, 135.4, 127.0, 126.5, 122.0, 121.7, 121.4, 115.7, 115.6, 110.8, 110.1, 96.6, 55.6; HRMS (MALDI-TOF): m/z $[M + H]^+$ calcd for $C_{21}H_{22}NO_5$, 368.1492, found 368.1491.

Synthesis of Cur-N-BF_2

Boron trifluoride etherate (426 mg, 3.0 mmol) was added into the THF solution (10 mL) of Cur-NH_2 (367 mg, 1.0 mmol), and the mixture was heated under reflux under nitrogen for 2 h. After completion of the reaction, the mixture was cooled to room temperature and evaporated under reduced pressure. The residue was then purified by silica gel column chromatography using dichloromethane as the eluent to afford a yellow solid of Cur-N-BF_2 in 31% yield (129 mg). ^{1}H NMR (DMSO-d_6, 500 MHz): δ 9.81 (s, 1H), 9.58 (d, J = 8.5 Hz, 2H), 7.77 (d, J = 16.0 Hz, 1H), 7.47 (d, J = 15.5 Hz, 1H), 7.31 (d, J = 2.0 Hz, 1H), 7.23 (d, J = 2.0 Hz, 1H), 7.13 (td, J_1 = 9.0 Hz, J_2 = 1.5 Hz, 2H), 6.88 (d, J = 8.5 Hz, 1H), 6.82 (t, J = 6.5 Hz, 1H), 6.78 (d, J = 5.5 Hz, 1H), 6.22 (d, J = 1.5 Hz, 1H), 3.84 (d, J = 2.0 Hz, 6H); ^{13}C NMR (DMSO-d_6, 125 MHz): δ 168.3, 166.1, 149.9, 149.0, 148.0, 147.9, 143.0, 138.7, 126.6, 126.0, 123.0, 122.5, 119.7, 118.2, 115.9, 115.7, 111.2, 111.0, 94.5, 55.6; HRMS (MALDI-TOF): m/z $[M + H]^+$ calcd for $C_{21}H_{20}BF_2NO_5$, 415.1397, found 415.1402.

Synthesis of Cur-O-BF_2

Boron trifluoride etherate (227 mg, 1.6 mmol) was added into the THF solution (10 mL) of curcumin (184 mg, 0.5 mmol), and the mixture was then heated under reflux overnight under nitrogen. The mixture was cooled to room temperature and then evaporated under reduced pressure. After addition of 10 mL hexane into to the residue, a red precipitate was obtained. After filtration and drying under a vacuum, Cur-O-BF_2 was obtained in 79% yield (164 mg). ^{1}H NMR (DMSO-d_6, 500 MHz): δ 10.12 (br s, 2H), 7.94 (s, 1H), 7.91 (s, 1H), 7.48 (d, J = 2.0 Hz, 2H), 7.35 (dd, J_1 = 8.5 Hz, J_2 = 1.5 Hz, 2H), 7.04 (s, 1H), 7.01 (s, 1H), 6.88 (d, J = 8.0 Hz, 2H), 6.46 (s, 1H), 3.86 (s, 6H); ^{13}C NMR (DMSO-d_6, 125 MHz): 178.7, 151.3, 148.2, 147.0, 126.0, 125.3, 117.9, 116.0, 112.4, 101.1, 55.8; HRMS (MALDI-TOF): m/z $[M + Na]^+$ calcd for $C_{21}H_{19}BF_2NaO_6$, 439.1135, found 439.1137.

Theoretical calculation method

The optimized molecular structures and molecular orbital amplitude plots of the HOMOs and LUMOs of Cur-N-BF_2 and Cur-O-BF_2 were calculated using density functional theory (DFT) at the B3LYP/6-31G(d,p) level with the Gaussian 09 package.

Fluorescence light-up detection of Aβ fibrils

The $A\beta_{1-42}$ fibrils were prepared according to a modified protocol reported in the literature.[20a] The $A\beta_{1-42}$ peptide (1.0 mg) was dissolved in hexafluoroisopropanol (0.22 mL) and then put in quiescence for 2 h. After sonication for 30 min to destroy the pre-existing aggregates, the solution was kept at −80 °C for 1.5 h and then lyophilized by vacuum freeze-drying to obtain a thin film at the bottom of the tube. The film was dissolved with DMSO (44.4 μL) to obtain a 5.0 mM stock solution and then diluted with PBS (4.396 mL) buffer to obtain 50 μM monomeric $A\beta_{1-42}$ solution, which was incubated at 37 °C for 0–7 days to induce the formation of $A\beta_{1-42}$ fibrils. The fluorescent probes of Cur-N-BF_2 (1.0 μL, 10 mM in DMSO) and ThT (1.0 μL, 10 mM in 80% ethanol and 20% PBS buffer) were respectively added into $A\beta_{1-42}$ solution (1.0 mL, 50 μM in PBS buffer) and the fluorescence signals were then measured with a multi-mode microplate reader. To further investigate the concentration effect of fluorescent probes for the detection of $A\beta_{1-42}$ fibrils, different concentrations (0–4.0 mM) of Cur-N-BF_2, curcumin, and ThT were respectively added into the solution of $A\beta_{1-42}$ fibrils (20 μM) and then the fluorescence intensities were measured with a microplate reader. To investigate the selectivity of Cur-N-BF_2 toward Aβ fibrils, the fluorescent probe of Cur-N-BF_2 (1.0 μL, 10 mM in DMSO) was added into $A\beta_{1-42}$ fibrils and human proteins [human serum albumin (HAS), transferrin, insulin, lysozyme, pepsin, and trypsin] (1.0 mL, 100 μg in PBS buffer) respectively and the fluorescence signals were then measured with a microplate reader.

Fluorescence imaging of Aβ plagues in brain slices

8 month-old double transgenic B6C3-Tg (APPswe, PSEN1dE9) 85Dbo/J (APP/PS1) mice and C57BL/6 mice (wild-type, WT) were obtained from Guangdong Medical Laboratory Animal Center (Guangdong, China). The mice were sacrificed under deep anesthesia using 10% chloral hydrate. The brain was removed and post-fixed in 4% paraformaldehyde. The brain tissue was

cryoprotected and stored in PB containing 30% sucrose, and then was cut into 20 μm serial sections in a coronal plane with a Leica SM2000R microtome (Leica Microsystems Inc., Nussloch, Germany). After mounting of tissue sections onto glass slides and drying overnight under air, the tissue sections were rehydrated with PBS (pH 7.4) for 5 min and then treated with H_2O_2 (3 wt%) for 10 min to inhibit endogenous peroxidase activity. After further washing with PBS three times, the brain tissue sections were incubated with 0.3% Triton X-100 at 37 °C for 1 h and then blocked with bovine serum albumin (BSA) at 37 °C for 1 h.

For staining with β-amyloid antibody, the brain tissue section was incubated with β-amyloid antibody (Cell Signaling Technology, 1:200) at 4 °C overnight. After washing and incubating with the secondary antibody (goat anti-rabbit IgG Rhodamine, 1:100) for 90 min at 37 °C, the sample was further washed with PBS three times and then was cover slipped with 50% glycerol. The fluorescence images were taken under a confocal microscope through irradiation at 543 nm with 50% laser power. The emission filter was 560–650 nm.

For staining with Cur-N-BF_2, the brain tissue section was incubated with 100 μM Cur-N-BF_2 at room temperature for 10 min and then cover slipped with 50% glycerol. The fluorescence images were taken under a confocal microscope through irradiation at 488 nm with 10% laser power. The emission filter was 500–620 nm.

For the co-staining experiment, the brain tissue section was first incubated with β-amyloid antibody (Cell Signaling Technology, 1:200) at 4 °C overnight and then washed with PBS three times. After incubation with the secondary antibody (goat anti-rabbit IgG Rhodamine, 1:100) for 90 min at 37 °C, the sample was washed with PBS three times and further incubated with 100 μM Cur-N-BF_2 at room temperature for 10 min. Then the sample was cover slipped with 50% glycerol and further imaged under a confocal microscope.

ThT fluorescence assay

The monomeric $A\beta_{1-42}$ (100 μM) in 1.0 mL PBS buffer was mixed with Cur-N-BF_2 (5.0 μL, 10 mM in DMSO). The monomeric $A\beta_{1-42}$ (100 μM) in 1.0 mL PBS buffer without Cur-N-BF_2 (addition of solvent only) was used as the control group. After incubation at 37 °C for predetermined time intervals, 20 μL of the incubation solutions containing $A\beta_{1-42}$ and "$A\beta_{1-42}$ + Cur-N-BF_2" were respectively mixed with 80 μL PBS buffer containing 10 μM ThT. The fluorescence intensity of ThT was then measured by a microplate reader. To explore the effects of Cur-N-BF_2 on the disassembly of Aβ fibrils, the monomeric $A\beta_{1-42}$ (100 μM) in 1.0 mL PBS buffer was incubated for 2 days at 37 °C to pre-form $A\beta_{1-42}$ fibrils and then was mixed with Cur-N-BF_2 (5.0 μL, 10 mM in DMSO). $A\beta_{1-42}$ pre-formed fibrils without Cur-N-BF_2 were used as the control group. After incubation at 37 °C for predetermined time intervals, 20 μL of the incubation solutions containing $A\beta_{1-42}$ fibrils and "$A\beta_{1-42}$ fibrils + Cur-N-BF_2" were respectively mixed with 80 μL PBS buffer containing 10 μM ThT. The fluorescence intensity of ThT was then measured by a microplate reader.

Cell viability

To investigate the optimum concentration of $A\beta_{1-42}$ fibrils for the *in vitro* AD cell model,[28] the differentiated HT22 cells were seeded in a 96-well plate at a density of 1×10^4 cells per well. After incubation at 37 °C for 24 h, the cells were exposed to different concentrations of $A\beta_{1-42}$ fibrils (0, 10, 20, and 40 μM) for 36 h to evaluate the cell viability by MTT assay.

The effect of Cur-N-BF_2 on $A\beta_{1-42}$-induced cytotoxicity was then evaluated by MTT assay. After incubation with 40 μM of $A\beta_{1-42}$ fibrils for 36 h, Cur-N-BF_2 (0, 5, 10 μM) was added into the culture media and further incubated for 24 h. MTT assay was then conducted to evaluate the cell viability of HT22 cells.

Cell morphology imaging

The effect of Cur-N-BF_2 on $A\beta_{1-42}$-induced cytotoxicity was also evaluated by observation of the cell morphological changes. The differentiated HT22 cells were seeded on cover slips in a 24-well plate at a density of 5×10^4 cells per well for 24 h, which were then treated with 40 μM $A\beta_{1-42}$ fibrils for 36 h. After further addition of 10 μM Cur-N-BF_2 and incubation for 24 h, the HT22 cells were then fixed on cover slips with 4% paraformaldehyde for 20 min, permeabilized with 0.1% Triton X-100 for 10 min, and blocked with BSA for 1h. The cells were then incubated with anti-tubulin antibody (abcam, 1:300) at 4 °C overnight. After washing and incubating with the secondary antibody (goat anti-rat IgG rhodamine, 1:50) for 90 min at 37 °C, the cells were washed with PBS three times and then stained with Hoechst 33342 for 10 min. The bright field and fluorescence images were then taken under a confocal microscope.

Conflicts of interest

There are no conflicts of interest to declare.

Acknowledgements

This work was financially supported by the National Science Foundation of China (21788102, 51620105009, 21877040, 21602063, and 81271476); the National Key R&D Program of China (2018YFC0311103); the Science and Technology Planning Project of Guangzhou (201704030069, 201607020015, and 201300000154); the 111 Project Grant (B13037); Pearl River S&T Nova Program of Guangzhou (201806010152); Natural Science Foundation of Guangdong Province (2013A030313852, 2013A030312002, and 2016A030313852); the Fundamental Research Funds for the Central Universities (2018JQ01); the Innovation and Technology Commission of Hong Kong (ITC-CNERC14SC01); and Guangdong Innovative Research Team Program (201101C0105067115).

Notes and references

1 N. A. Bishop, T. Lu and B. A. Yankner, *Nature*, 2010, **464**, 529–535.
2 A. Kontush, *Free Radical Biol. Med.*, 2001, **31**, 1120–1131.

3 P. B. Rosenberg, D. F. Wong, S. L. Edell, J. S. Ross, A. D. Joshi, J. R. Brasic, Y. Zhou, V. Raymont, A. Kumar, H. T. Ravert, R. F. Dannals, M. J. Pontecorvo, D. M. Skovronsky and C. G. Lyketsos, *Am. J. Geriat. Psychiat.*, 2013, **21**, 272–278.

4 X. Zhang, Y. Hou, C. Peng, C. Wang, X. Wang, Z. Liang, J. Lu, B. Chen, J. Dai, B. Liu and M. Cui, *J. Med. Chem.*, 2018, **61**, 1330–1339.

5 C. C. Rowe, K. A. Ellis, M. Rimajova, P. Bourgeat, K. E. Pike, G. Jones, J. Fripp, H. Tochon-Danguy, L. Morandeau, G. O'Keefe, R. Price, P. Raniga, P. Robins, O. Acosta, N. Lenzo, C. Szoeke, O. Salvado, R. Head, R. Martins, C. L. Masters, D. Ames and V. L. Villemagne, *Neurobiol. Aging*, 2010, **31**, 1275–1283.

6 M. M. Xu, W. M. Ren, X. C. Tang, Y. H. Hu and H. Y. Zhang, *Acta Pharmacol. Sin.*, 2016, **37**, 719–730.

7 (*a*) W. T. Dou, W. Chen, X. P. He, J. Su and H. Tian, *Faraday Discuss.*, 2017, **196**, 395–402; (*b*) A. C. Sedgwick, W. T. Dou, J. B. Jiao, L. Wu, G. T. Williams, A. Jenkins, S. D. Bull, J. L. Sessler, X. P. He and T. D. James, *J. Am. Chem. Soc.*, 2018, **140**, 14267–14271; (*c*) H. Tong, K. Lou and W. Wang, *Acta Pharm. Sin. B*, 2015, **5**, 25–33.

8 (*a*) P. Hanczyc, L. Sznitko, C. Zhong and A. J. Heeger, *ACS Photonics*, 2015, **2**, 1755–1762; (*b*) N. D. Younan and J. H. Viles, *Biochemistry*, 2015, **54**, 4297–4306.

9 (*a*) M. Gao and B. Z. Tang, *ACS Sens.*, 2017, **2**, 1382–1399; (*b*) J. Mei, N. L. Leung, R. T. Kwok, J. W. Lam and B. Z. Tang, *Chem. Rev.*, 2015, **115**, 11718–11940; (*c*) J. Liang, B. Z. Tang and B. Liu, *Chem. Soc. Rev.*, 2015, **44**, 2798–2811; (*d*) R. T. Kwok, C. W. Leung, J. W. Lam and B. Z. Tang, *Chem. Soc. Rev.*, 2015, **44**, 4228–4238; (*e*) J. Qian and B. Z. Tang, *Chem*, 2017, **3**, 56–91; (*f*) Y. Hong, J. W. Lam and B. Z. Tang, *Chem. Soc. Rev.*, 2011, **40**, 5361–5388; (*g*) Y. Yuan, G. Feng, W. Qin, B. Z. Tang and B. Liu, *Chem. Commun.*, 2014, **50**, 8757–8760; (*h*) X. Ou, X. Lou and F. Xia, *Sci. China: Chem.*, 2017, **60**, 663–669.

10 (*a*) J. Qi, C. Chen, X. Zhang, X. Hu, S. Ji, R. Kwok, J. Lam, D. Ding and B. Z. Tang, *Nat. Commun.*, 2018, **9**, 1848; (*b*) X. Ni, X. Zhang, X. Duan, H. Zheng, X. Xue and D. Ding, *Nano Lett.*, 2018, **19**, 318–330; (*c*) H. Gao, X. Zhang, C. Chen, K. Li and D. Ding, *Adv. Biosyst.*, 2018, **2**, 1800074; (*d*) W. T. Dou, J. J. Zhang, Q. Li, Z. Guo, W. Zhu, G. R. Chen, H. Y. Zhang and X. P. He, *ChemBioChem*, 2018, DOI: 10.1002/cbic.201800508.

11 (*a*) Y. Hong, L. Meng, S. Chen, C. W. Leung, L. T. Da, M. Faisal, D. A. Silva, J. Liu, J. W. Lam, X. Huang and B. Z. Tang, *J. Am. Chem. Soc.*, 2012, **134**, 1680–1689; (*b*) N. Pradhan, D. Jana, B. K. Ghorai and N. R. Jana, *ACS Appl. Mater. Interfaces*, 2015, **7**, 25813–25820; (*c*) R. R. Hu, E. Lager, A. Aguilar-Aguilar, J. Z. Liu, J. W. Y. Lam, H. H. Y. Sung, I. D. Williams, Y. C. Zhong, K. S. Wong, E. Pena-Cabrera and B. Z. Tang, *J. Phys. Chem. C*, 2009, **113**, 15845–15853; (*d*) W. Fu, C. Yan, Z. Guo, J. Zhang, H. Zhang, H. Tian and W.-H. Zhu, *J. Am. Chem. Soc.*, 2019, **141**, 3171–3177.

12 (*a*) D. S. Kim, S. Y. Park and J. K. Kim, *Neurosci. Lett.*, 2001, **303**, 57–61; (*b*) F. Yang, G. P. Lim, A. N. Begum, O. J. Ubeda, M. R. Simmons, S. S. Ambegaokar, P. P. Chen, R. Kayed, C. G. Glabe, S. A. Frautschy and G. M. Cole, *J. Biol. Chem.*, 2005, **280**, 5892–5901; (*c*) M. Garcia-Alloza, L. A. Borrelli, A. Rozkalne, B. T. Hyman and B. J. Bacskai, *J. Neurochem.*, 2007, **102**, 1095–1104; (*d*) X. Zhang, Y. Tian, P. Yuan, Y. Li, M. A. Yaseen, J. Grutzendler, A. Moore and C. Ran, *Chem. Commun.*, 2014, **50**, 11550–11553.

13 (*a*) A. Belkacemi, S. Doggui, L. Dao and C. Ramassamy, *Expert Rev. Mol. Med.*, 2011, **13**, e34; (*b*) K. G. Goozee, T. M. Shah, H. R. Sohrabi, S. R. Rainey-Smith, B. Brown, G. Verdile and R. N. Martins, *Br. J. Nutr.*, 2016, **115**, 449–465; (*c*) X. Zhang, Y. Tian, C. Zhang, X. Tian, A. W. Ross, R. D. Moir, H. Sun, R. E. Tanzi, A. Moore and C. Ran, *Proc. Natl. Acad. Sci. U. S. A.*, 2015, **112**, 9734–9739; (*d*) C. Gan, J. Hu, D. D. Nan, S. Wang and H. Li, *Future Med. Chem.*, 2017, **9**, 1587–1596; (*e*) D. Chin, P. Huebbe, K. Pallauf and G. Rimbach, *Curr. Med. Chem.*, 2013, **20**, 3955–3985.

14 C. Ran, X. Xu, S. B. Raymond, B. J. Ferrara, K. Neal, B. J. Bacskai, Z. Medarova and A. Moore, *J. Am. Chem. Soc.*, 2009, **131**, 15257–15261.

15 (*a*) R. Yoshii, A. Hirose, K. Tanaka and Y. Chujo, *Chem. – Eur. J.*, 2014, **20**, 8320–8324; (*b*) M. Yamaguchi, S. Ito, A. Hirose, K. Tanaka and Y. Chujo, *Mater. Chem. Front.*, 2017, **1**, 1573–1579; (*c*) R. Yoshii, K. Suenaga, K. Tanaka and Y. Chujo, *Chem. – Eur. J.*, 2015, **21**, 7231–7237.

16 (*a*) R. Hu, E. Lager, A. Aguilar-Aguilar, J. Liu, J. W. Y. Lam, H. H. Y. Sung, I. D. Williams, Y. Zhong, K. S. Wong, E. Pena-Cabrera and B. Z. Tang, *J. Phys. Chem. C*, 2009, **113**, 15845–15853; (*b*) M. Jiang, X. Gu, J. Lam, Y. Zhang, R. Kwok, K. S. Wong and B. Z. Tang, *Chem. Sci.*, 2017, **8**, 5440–5446; (*c*) K. Li, Y. Liu, Y. Li, Q. Feng, H. Hou and B. Z. Tang, *Chem. Sci.*, 2017, **8**, 7258–7267; (*d*) M. Gao, H. Su, Y. Lin, X. Ling, S. Li, A. Qin and B. Z. Tang, *Chem. Sci.*, 2017, **8**, 1763–1768; (*e*) M. Gao, H. Su, S. Li, Y. Lin, X. Ling, A. Qin and B. Z. Tang, *Chem. Commun.*, 2017, **53**, 921–924.

17 M. A. Haidekker, T. P. Brady, D. Lichlyter and E. A. Theodorakis, *Bioorg. Chem.*, 2005, **33**, 415–425.

18 R. Yoshii, A. Nagai, K. Tanaka and Y. Chujo, *Chem. – Eur. J.*, 2013, **19**, 4506–4512.

19 (*a*) S. Fan, Y. Zheng, X. Liu, W. Fang, X. Chen, W. Liao, X. Jing, M. Lei, E. Tao, Q. Ma, X. Zhang, R. Guo and J. Liu, *Drug Delivery*, 2018, **25**, 1091–1102; (*b*) H. Y. Zhang, C. Y. Sun, M. Adu-Frimpong, J. N. Yu and X. M. Xu, *Int. J. Pharm.*, 2018, **555**, 270–279; (*c*) N. S. Rejinold, P. R. Sreerekha, K. P. Chennazhi, S. V. Nair and R. Jayakumar, *Int. J. Biol. Macromol.*, 2011, **49**, 161–172.

20 (*a*) W. B. Stine, L. Jungbauer, C. Yu and M. J. LaDu, *Methods Mol. Biol.*, 2011, **670**, 13–32; (*b*) H. R. Levine, *Protein Sci.*, 1993, **2**, 404–410.

21 (*a*) M. T. Heneka, M. P. Kummer, A. Stutz, A. Delekate, S. Schwartz, A. Vieira-Saecker, A. Griep, D. Axt, A. Remus, T. C. Tzeng, E. Gelpi, A. Halle, M. Korte, E. Latz and D. T. Golenbock, *Nature*, 2013, **493**, 674–678; (*b*) P. Yan, A. W. Bero, J. R. Cirrito, Q. Xiao, X. Hu, Y. Wang, E. Gonzales, D. M. Holtzman and J. M. Lee, *J. Neurosci.*, 2009, **29**, 10706–10714.

22 J. M. Collins, A. E. King, A. Woodhouse, M. T. Kirkcaldie and J. C. Vickers, *Exp. Neurol.*, 2015, **267**, 219–229.

23 (*a*) H. Kim, B. S. Park, K. G. Lee, C. Y. Choi, S. S. Jang, Y. H. Kim and S. E. Lee, *J. Agric. Food Chem.*, 2005, **53**, 8537–8541; (*b*) M. Moon, H. Song, H. J. Hong, D. W. Nam, M. Cha, M. S. Oh, J. Yu, H. Ryu and I. Mook-jung, *Cell Death Differ.*, 2013, **20**, 630–638.

24 (*a*) F. Yang, G. P. Lim, A. N. Begum, O. J. Ubeda, M. R. Simmons, S. S. Ambegaokar, P. P. Chen, R. Kayed, C. G. Glabe, S. A. Frautschy and G. M. Cole, *J. Biol. Chem.*, 2005, **280**, 5892–5901; (*b*) D. Yanagisawa, H. Taguchi, A. Yamamoto, N. Shirai, K. Hirao and I. Tooyama, *J. Alzheimer's Dis.*, 2011, **24**, 33–42.

25 M. Bartolini, C. Bertucci, M. L. Bolognesi, A. Cavalli, C. Melchiorre and V. Andrisano, *ChemBioChem*, 2007, **8**, 2152–2161.

26 (*a*) K. Rajasekhar, S. N. Suresh, R. Manjithaya and T. Govindaraju, *Sci. Rep.*, 2015, **5**, 8139; (*b*) B. J. Blanchard, A. Chen, L. M. Rozeboom, K. A. Stafford, P. Weigele and V. M. Ingram, *Proc. Natl. Acad. Sci. U. S. A.*, 2004, **101**, 14326–14332.

27 (*a*) J. Liu, L. Li and W. Z. Suo, *Life Sci.*, 2009, **84**, 267–271; (*b*) P. H. Reddy, M. Manczak, X. Yin, M. C. Grady, A. Mitchell, R. Kandimalla and C. S. Kuruva, *J. Invest. Med.*, 2016, **64**, 1220–1234.

28 (*a*) M. Wu, J. Jia, C. Lei, L. Ji, X. Chen, H. Sang and L. Xiong, *J. Mol. Neurosci.*, 2015, **55**, 778–787; (*b*) P. Gonzalez, K. Pota, L. S. Turan, C. V. Da, G. Akkaraju and K. N. Green, *ACS Chem. Neurosci.*, 2017, **8**, 2414–2423; (*c*) L. Chen, S. Ou, L. Zhou, H. Tang, J. Xu and K. Guo, *Neurosci. Lett.*, 2017, **639**, 36–42.